APPLICATION OF INTERFACE TECHNOLOGY IN NONLINEAR ANALYSIS OF A STITCHED/RFI COMPOSITE WING STUB BOX

John T. Wang* and Jonathan B. Ransom*

NASA Langley Research Center, Hampton, VA

Abstract

A recently developed interface technology was successfully employed in the geometrically nonlinear analysis of a full-scale stitched/RFI composite wing box loaded in bending. The technology allows mismatched finite element models to be joined in a variationally consistent manner and reduces the modeling complexity by eliminating transition meshing. In the analysis, local finite element models of nonlinearly deformed wide bays of the wing box are refined without the need for transition meshing to the surrounding coarse mesh. The COMET-AR finite element code, which has the interface technology capability, was used to perform the analyses. The COMET-AR analysis is compared to both a NASTRAN analysis and to experimental data. The interface technology solution is shown to be in good agreement with both. The viability of interface technology for coupled global/local analysis of large scale aircraft structures is demonstrated.

Introduction

The wing stub box, see Figures 1 and 2, represents the inboard portion of a high-aspect-ratio wing box for a future civil-transport-aircraft. It was designed and manufactured by the McDonnell Douglas Aerospace Company under the NASA Advanced Composites Technology Program. The fabrication employs an innovative stitched/RFI manufacturing process which has the potential for reducing manufacturing costs and producing damage-tolerant composite primary aircraft structures. Test results for the wing stub box[1] reveal that large nonlinear deformations exist in the wide bays outboard of the upper-cover access door when the test article is subjected to upbending. Investigations[2] following the test show that mesh refinement of the initial (pretest) finite element model in the wide bays of the stub box is required to accurately account for nonlinear deformations. To connect the refined mesh region to the surrounding coarse mesh region, conventional transition meshing can be used. However, transition meshing usually creates triangular and/or badly distorted quadrilateral elements which cause modeling complexity and deteriorate solution accuracy. Instead of using a transition mesh, the interface technology[3,4] can be used to connect the refined mesh region directly to the coarse region without remeshing the common boundaries of the two regions. Using this technology (see the Appendix for a brief description of the formulation), the matching of nodes at the common boundary of the refined and coarse mesh regions is not needed. Considering a design process in which critical (local) regions may need remeshing many times due to various design changes, the elimination of transition meshing between the critical (local) regions and the noncritical (global) regions can significantly improve modeling efficiency and hence shorten the design time.

Application of the interface technology to linear structural analyses has been investigated and its advantages over conventional transition meshing have been documented.[3,4,6,7] However, the use of this technology on complex structures undergoing large nonlinear behavior has not been investigated. The objective of this paper is to apply the interface technology in a geometrically nonlinear analysis of the McDonnell Douglas wing-stub-box test article using a procedure recently developed by Ransom.[5] Finite element analysis results from the interface technology model are compared herein with NASTRAN results[2] and with experimental data.[8]

Wing-Stub-Box Test Article

The wing-stub-box test article consists of an inboard metallic load-transition structure at the wing root, the composite wing stub box, and an outboard metallic extension structure from the composite wing stub box out to the wing tip. A photograph of the test article in the NASA Langley Research Center Structural Mechanics Test Laboratory is shown in Figure 1. As shown in Figure 2, the composite wing stub box is approximately twelve feet long and eight feet wide. The maximum box depth at the root of the composite wing stub box is approximately 2.3 feet. The load-transition

---

* Aerospace Engineer, CSB/SD, Member AIAA

structure is located inboard of the composite wing stub box (between the composite wing stub box and the vertical reaction structure at the wing-stub-box root). The wing-tip extension structure is located outboard of the composite wing stub box. The load-transition structure is mounted to a steel and concrete vertical reaction structure resulting in a near-clamped end condition.

The composite wing stub box was fabricated by using an innovative RFI process.[9] AS4/3501-6 and IM7/3501-6 graphite-epoxy materials (Hercules, Inc.) were stitched together using Kevlar thread (E. I. DuPont de Nemours, Inc.). IM7 graphite fibers were used only for the 0-degree fibers in the lower cover panel skin. As shown in Figures 3 and 4, the composite wing stub box consists of ribs, spars, and upper and lower cover panels. The stringers and intercostals were stitched to the cover panels. The stub box was subjected to a series of tests at the NASA Langley Research Center's Structural Mechanics Test Laboratory. In the final test, the wing stub box was loaded to failure after the infliction of a 100 ft-lb impact damage at a critical location. The final failure load was 154 kips.

Finite Element Models and Analysis Codes

Analytical results presented in this paper were obtained from two finite element models, the NASTRAN model and the COMET-AR interface technology model. These models are refined versions of the initial finite element model shown in Figure 5. The NASTRAN model and the interface technology model are shown in Figures 6 and 8, respectively. The primary differences between the NASTRAN model and the initial model are that; (a) the mesh density of the wide bays of the upper-cover-panel skin outboard of the access door are increased, and (b) the blade stringers are modeled as plate elements in place of the beam elements used in the initial model (see Figures 6 and 7). Note that the refined region in Figure 6 is connected to the outside coarse mesh region using a transition mesh. The process of transition meshing, in which the skin, stiffeners and ribs need to be remeshed, is complex (see Figures 6 and 7). In addition, many elements in the resulting transition mesh are distorted (hence, accuracy may be compromised.) The transition mesh is eliminated in the interface technology model shown in Figure 8. The refined region is directly connected to the coarse region using interface elements[4,5] as discussed in the Appendix.

Solution sequence 106 of the MSC/NASTRAN[10] finite element code, Version 68, was used to perform the geometrically nonlinear analysis with the NASTRAN model. The COMET-AR[11] code was used to perform the nonlinear analysis with the interface technology model (see Appendix for nonlinear analysis with interface technology). Quadrilateral AQ4 shell elements[12] with drilling degrees of freedom, triangular MIN3 elements[13], and two-noded beam E210 elements[14] were used in the COMET-AR analysis. MSC/PATRAN[15] was used to create the models and to postprocess the analytical results.

Analysis Results

Analytical results from the interface technology model are compared with the NASTRAN results and the experimental data. Correlation plots of displacement and strains are presented.

Correlation of displacements

The predicted deformed shapes of the composite stub box from the NASTRAN model and the interface technology model are shown in Figures 9 and 10 for the case of failure loading (154 kips). The relatively large out-of-plane deformation in the upper cover panel outboard from the access door shown in both figures is caused by the lack of longitudinal support in this region. Analytical predictions and experimental results for the vertical displacements, measured by Direct Current Differential Transformers (DCDT's), at six locations on the bottom surface of the stub box and at the wing tip are shown in Figures 11-13. These figures show the variation of vertical displacements with the applied load at the wing tip. Rigid body motions of the load-transition structure relative to the vertical reaction structure were removed from the measured data to obtain the results presented in these figures. Tip and bottom surface displacement results from the NASTRAN analysis and the COMET-AR interface technology analysis were found to be within 1% of each other. At the wing tip, the difference between the experimental and the analytical results is approximately 6 %, as shown in Figure 11. Measurements at three locations along the rear spar are shown in Figure 12, and measurements at three locations along the front spar are shown in Figure 13. The correlation between the analytical results and the experimental results at these six locations is considered to be good for such a large, complex test article.

Correlation of strains

Analytical and experimental axial strains for strain gages 17, 20, and 84 are plotted in Figures 14-16. The axial direction is parallel to the rear spar of the wing stub box. These strain gages are located sufficiently far from the access-door cutout and the nonlinearly deformed region to be considered as far field results. In Figures 14-16 and 19-22, the hatched region in the sketch of the wing stub box is the mesh refinement region. The correlation plots in Figures 14-16 indicate that the far

field strains predicted by the analysis are reasonably accurate.

Circumferential strain results on the external surface of the upper-cover-panel skin at the edge of the access-door cutout, measured by strain gages 78 and 79, are shown in Figures 17 and 18. Analytical and experimental results for these external strain gages indicate approximately linear behavior. Results from the interface technology model are in good agreement with NASTRAN predictions and experimental data.

Predicted and measured axial strain results for the first and second bays outboard of the access-door cutout of the upper cover panel are shown in Figures 19-21. The first and second bays are 18 inches wide, and had nonlinear deformations due to the lack of longitudinal stiffeners. Results for; (a) strain gages 67 and 68 on the upper-cover-panel skin in the first bay, immediately outboard from the access door are shown in Figure 19, (b) strain gages 63 and 64 on the upper-cover-panel skin in the second bay outboard of the access door are shown in Figure 20, and (c) strain gages 22-24 at the edge of this bay are shown in Figure 21. In general, good correlation was obtained between experimental and analytical results in the skin and on the stiffeners for the first and second bays outboard of the access door, as shown in Figures 19-21. This indicates the interface technology model and the NASTRAN model can reliably predict strains in these two nonlinearly deformed bays. Predicted and measured strain results for strain gages 49 and 50, located at the center of the third bay bays outboard of the access-door cutout on a discontinuous stiffener (see Figure 3), are also shown in Figure 22. The correlation between experimental and analytical strain results shown is acceptable.

Concluding Remarks

Interface technology is successfully employed in the geometrically nonlinear analysis of a full-scale stitched/RFI composite wing stub box loaded in bending. In the interface technology model, local nonlinearly deformed wide bays are refined and interface elements are used in connecting the refined region to the surrounding coarse mesh region. The interface technology model is analyzed using the COMET-AR finite element code. Results from the interface technology model are compared with results from a NASTRAN model and experimental data. The interface technology model results are in good agreement with both the NASTRAN results and the experimental data. The advantages of using interface technology in connecting a refined local region to a unrefined global region are evident when comparing the interface technology model with the NASTRAN model. Transition meshing as used in the NASTRAN model and the possible errors arising from the distorted elements used in the transition meshing region are eliminated. This paper clearly demonstrates that the use of interface technology can substantially reduce the modeling effort required to couple local refined finite element models to coarse global models in the analysis of large scale aircraft structures.

Acknowledgement

The authors wish to acknowledge the PATRAN modeling and COMET-AR support provided by Brian Mason and Christine Lotts of Analytical Services and Materials, Inc.

References

1. Hinrichs, S. C., Jegley, D. C., and Wang, J. T., "Structural Analysis and Test of a Stitched Composite Wing Box," Presented in the *6th NASA/DoD Advanced Composite Technology Conference*, Anaheim, CA, August 7-11, 1995.

2. Wang, J. T., Jegley, D. C., Bush, H. G., and Hinrichs, S. C., *Correlation of Structural Analysis and Test Results for the McDonnell Douglas Stitched/RFI All-Composite Wing Stub Box*, NASA TM-110267, July 1996.

3. Aminpour, M. A., Ransom, J. B., and McCleary, S. L., "Coupled Analysis of Independently Modeled Finite Element Subdomains," *33rd AIAA/ ASME/ASCE/AHS/ASC Structures, Structural Dynamics, and Materials Conference*, AIAA-92-2235-CP, 1992.

4. Ransom, J. B., McCleary S. L., and Aminpour, M. A., "A New Interface Element for Connecting Independently modeled Substructures," *34th AIAA/ASME/ASCE/AHS/ASC Structures, Structural Dynamics, and Materials Conference*, AIAA-93-1503-CP, 1993.

5. Ransom, J. B., "Interface Technology for Geometrically Nonlinear Analysis of Multiple Connected Subdomains," to be published as AIAA-97-1298-CP, 1997.

6. Aminpour, M. A., Krishnamurthy T., McClearly S. L., and Baddourah, M. A., "Application of New Interface Element to the Global/Local Analysis of a Boeing Composite Crown Panel," *Proceedings of the Fourth NASA/DoD Advanced Composites Technology Conference*, NASA CP 3229, pp. 773-788, 1993.

7. Housner, J. M., Aminpour, M. A., Davila, C. G., Schiermeier, J. E., Stroud, W. J., Ransom, J. B., Gillian, R. E., "An Interface Element for Global/Local and Substructuring Analysis,"

Presented at MSC World Users' Conference, Los Angles, CA, May 8-12, 1995.

8. Jegley, D. C. and Bush, H. G., *Test Documentation and Results of the Structural Tests on the All-Composite McDonnell Douglas Wing Stub Box*, NASA TM 110204, April 1996.

9. Markus, A. M., Thrash, P., and Grossheim, B. G., "Manufacturing Development and Requirements for Stitched/RTM Wing Structure," *Proceedings of the Fourth NASA/DoD Advanced Composites Technology Conference*, NASA CP 3229, pp. 503-523, 1993.

10. *MSC/NASTRAN Quick Reference Guide*, Version 68, edited by Reymond, M. and Miller M., The MacNeal-Schwendler Corporation, February 1994.

11. Stanley, G. M., Hurbut, B., Levit, I., Stehlin, B., Loden, W., and Swenson, L., *COMET-AR Adaptive Refinement Manual*, LMSC Report #F318482, 1991

12. Aminpour, M. A., "An Assumed-Stress Hybrid 4-Node Shell Element with Drilling Degrees of Freedom,' *International Journal for Numerical Methods in Engineering*, Vol. 33, pp. 19-38, 1992.

13. Tessler, A., "A C°-anisoparametric three-node shallow shell element," *Computer Methods in Applied Mechanics and Engineering*, Vol. 78, pp. 89-103, 1990.

14. Nour-Omid, S., Brogan F. A., Stanley, G. M., *The Computational Structural Mechanics Testbed Structural Element Processor ES6: STAGS Beam Element*, NASA CR-4359, May 1991.

15. Anon., *MSC/PATRAN V5.0 Release Notes*, The MacNeal-Schwendler Corporation Publication No. 903057, March 1996.

16. Rankin, C. C., and Brogan, F. A.: "An Element-Independent Corotational Procedure for the Treatment of Large Rotations." In *Collapse Analysis of Structures*, edited by , L. H. Sobel and K. Thomas, ASME, New York, pp. 85-100, 1984.

17. Riks, E., "On the Numerical Solution of Snapping Problems in the Theory of Stability," August 1970, Stanford University, SUDAAR Report No. 401. Also available as AFOSR Report No. 70-2258TR.

18. Wempner, G. A., "Discrete Approximations Related to Nonlinear Theories of Solids," *International Journal of Solids and Structures*, Vol. 7, pp. 1581-1589, 1971.

19. Crisfield, M. A., *Non-linear Finite Element Analysis of Solids and Structures*, Vol. 1, John Wiley & Sons, ISBN 0 471 92956 5(v.1), 1991.

Appendix - Interface Technology

Recently, a method for connecting finite element models without the use of transition modeling has been developed[3,4]. This method, called interface technology, is an improved technique for connecting multiple dissimilar meshed subdomains or substructures to form a single finite element model. It is based on employing interface elements that make use of a hybrid variational formulation to provide for compatibility between independently modeled subdomains.

The interface element for linear and nonlinear analyses was developed in detail in references 4 and 5, respectively. The formulation for nonlinear analysis and the associated nonlinear solution strategy are briefly described, herein. It allows the independent modeling of different substructures or components without concern for one-to-one nodal coincidence between the finite element models. Moreover, it acts as "mathematical glue" between independent finite element models with different mesh densities and nodal layouts. It is based on an analytical variational procedure and avoids the use of transition meshes.

Interface Element Formulation

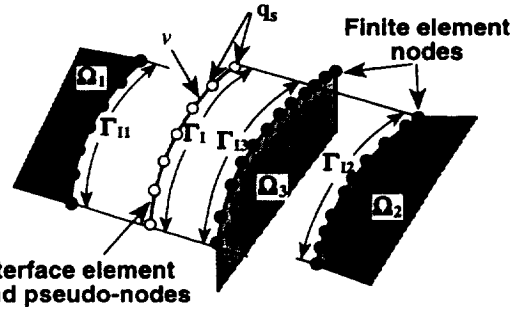

Figure A-1. Typical Interface Element Definition.

Consider the three independently discretized substructures shown in Figure A-1. The interface element is discretized with a mesh of evenly-spaced pseudo-nodes (open circles in the figure) which need not be coincident with any of the interface nodes (filled circles in the figure) of any of the substructures. The hybrid variational formulation[3,4] employs an integral form for the compatibility between the interface line element and the finite element substructures. The displacement vector, v, of the interface element is assumed to be independent of the displacement vectors, u, of the substructures to which it is attached. The weak form of the principle of virtual work leads to a modified virtual work expression which may be written as

$$\delta\overline{W} = \sum_{k=1}^{N_{ss}} \delta W_k + \sum_{i=1}^{N_I} \delta W_{c_i} = 0 \tag{1}$$

where N_{ss} is the total number of substructures and N_I is the total number of interface elements.

For the k^{th} substructure,

$$\delta W_k = \delta q_k^T (K_T)_k q_k - \delta q_k^T f_k \tag{2}$$

and

$$f_k = \int_{\Omega_k} N_k^T F_k \, d\Omega_k + \int_{S_k^{(\sigma)}} N_k^T \phi_k \, dS_k^{(\sigma)} \tag{3}$$

where $(K_T)_k$ is the tangent stiffness matrix, N_k are the finite element shape functions, δq_k are the variations of generalized displacements, q_k, F_k are the external applied forces, and ϕ_k are the applied tractions on the subdomain boundary, $S_k^{(\sigma)}$.

The compatibility between interface element i and its connecting substructures is enforced through the use of the constraint integral

$$\delta W_{c_i} = \sum_{j=1}^{n_{ss}(i)} \left\{ \begin{array}{l} \int_{\Gamma_{ij}} \delta\lambda_{ij}^T \left(v_i - u_{ij} \right) d\Gamma_{ij} - \\ \int_{\Gamma_{ij}} \delta u_{ij}^T \lambda_{ij} \, d\Gamma_{ij} + \int_{\Gamma_{ij}} \delta v_i^T \lambda_{ij} \, d\Gamma_{ij} \end{array} \right\} \tag{4}$$

where $n_{ss}(i)$ is the number of substructures connected to the interface element i, u_{ij} are the displacements at the boundary of substructure j connected to interface element i, and v_i are the displacements of the interface element i, and λ_{ij} are the Lagrange multipliers.

The independent approximations for the finite element displacements, interface displacements, and interface tractions are, respectively

$$\begin{aligned} u_{ij} &= N_{ij} \bar{q}_{ij} \\ v_i &= T_i q_{s_i} \\ \lambda_{ij} &= R_{ij} \alpha_{ij} \end{aligned} \tag{5}$$

where $\bar{q}_{ij}$ and q_{s_i} are the nodal degrees of freedom corresponding to u_{ij} and v_i, and α_{ij} are the unknown coefficients of the Lagrange multipliers, λ_{ij}. The matrix N_{ij} is the matrix of finite element shape functions on substructure j along interface i, T_i is formed as a result of passing a cubic spline through the evenly-spaced pseudo-nodes, R_{ij} is formed as a result of using constant functions for linear finite elements and linear functions for quadratic finite elements.

The interface matrices may be defined as

$$M_{ij} = -\int_{\Gamma_{ij}} N_{ij}^T R_{ij} \, d\Gamma_{ij} \text{ and } G_{ij} = \int_{\Gamma_{ij}} T_i^T R_{ij} \, d\Gamma_{ij} \tag{6}$$

Thus, for arbitrary q_k on Ω_k, arbitrary q_{s_i} on Γ_I and arbitrary α_{ij} on Γ_I, the interface element system of equations is given as

$$\begin{bmatrix} K_T & 0 & M_I \\ 0 & 0 & G_I \\ M_I^T & G_I^T & 0 \end{bmatrix} \begin{Bmatrix} q \\ q_s \\ \alpha \end{Bmatrix} = \begin{Bmatrix} f \\ 0 \\ 0 \end{Bmatrix} \tag{7}$$

where K_T, q and f are the assembled tangent stiffness matrix, displacement vector and force vector for the entire structure, and M_I, G_I, q_s and α are the assembled M_{ij}, G_{ij}, q_{s_i}, and α_{ij} for all interface elements.

Nonlinear Solution Strategy

The nonlinear solution procedure employed herein is based on an automatic load incremental control and the Newton/Raphson iteration method. The so-called modified Newton/Raphson method, which forms and factors the tangent stiffness matrix periodically rather than at every nonlinear iteration, has been used in the nonlinear analysis of the wing stub box. A corotational formulation[16] which identifies the reference state as the current deformed configuration is used to describe the motion. This formulation separates the rigid body motion from the strain-producing motion thus allowing for either linear or nonlinear strain-displacement relations at the finite element level. Strain-producing deformations are computed based on the original configuration within the local corotated frame. An arc-length control strategy[17,18,19] is used for automatic load incremental control to obtain the load-deflection response and to handle limit points. This nonlinear solution strategy has been adapted to incorporate the interface element[5] and was implemented within a general-purpose, finite element code COMET/AR.[11]

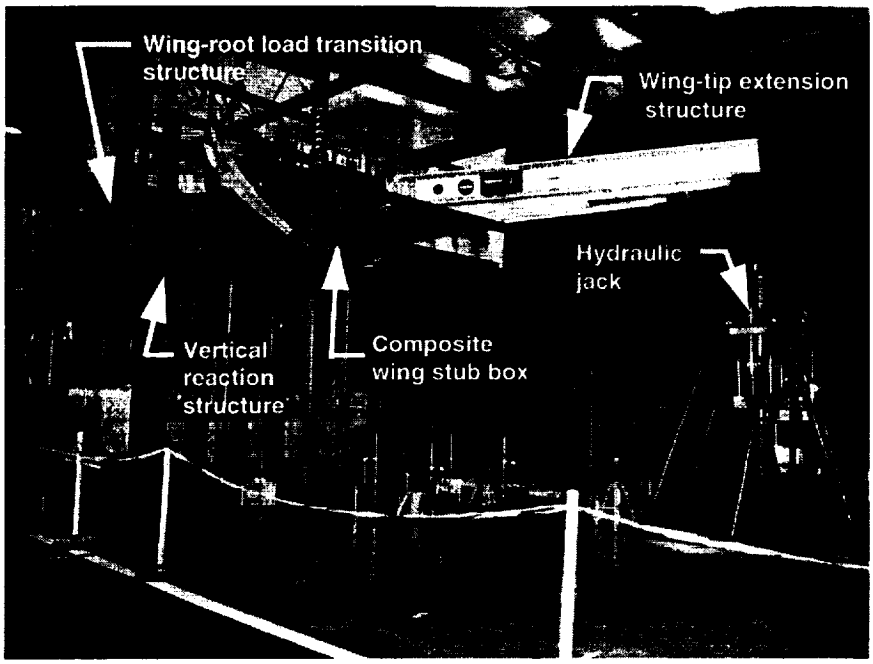

Figure 1. Wing-stub-box test article attached to the vertical reaction structure.

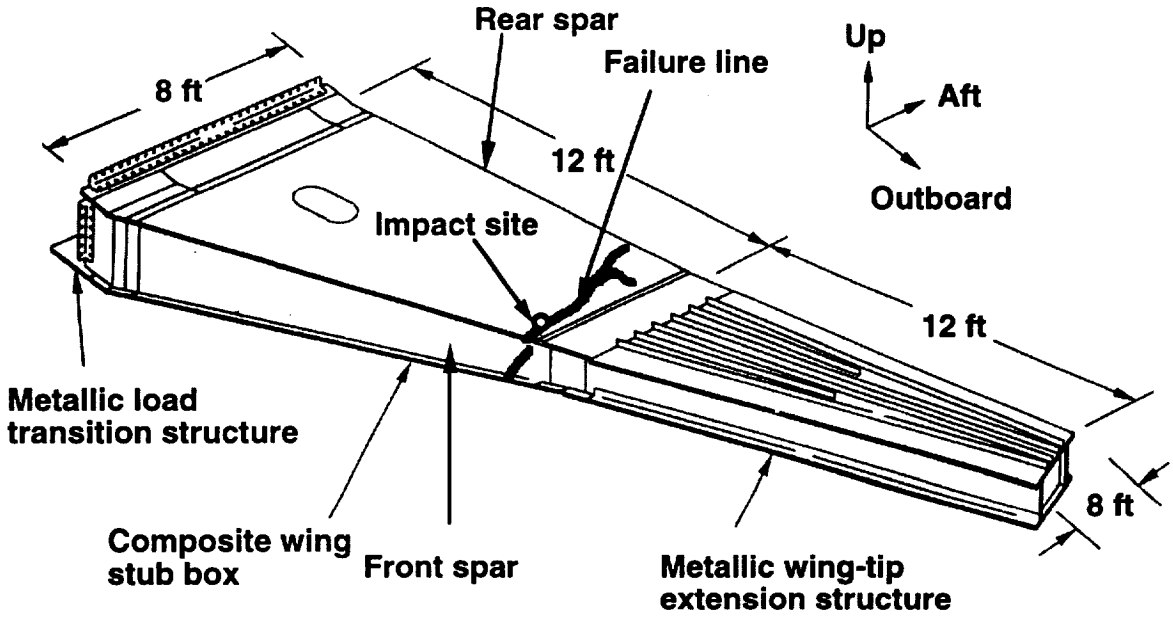

Figure 2. Dimensions of the wing-stub box test article.

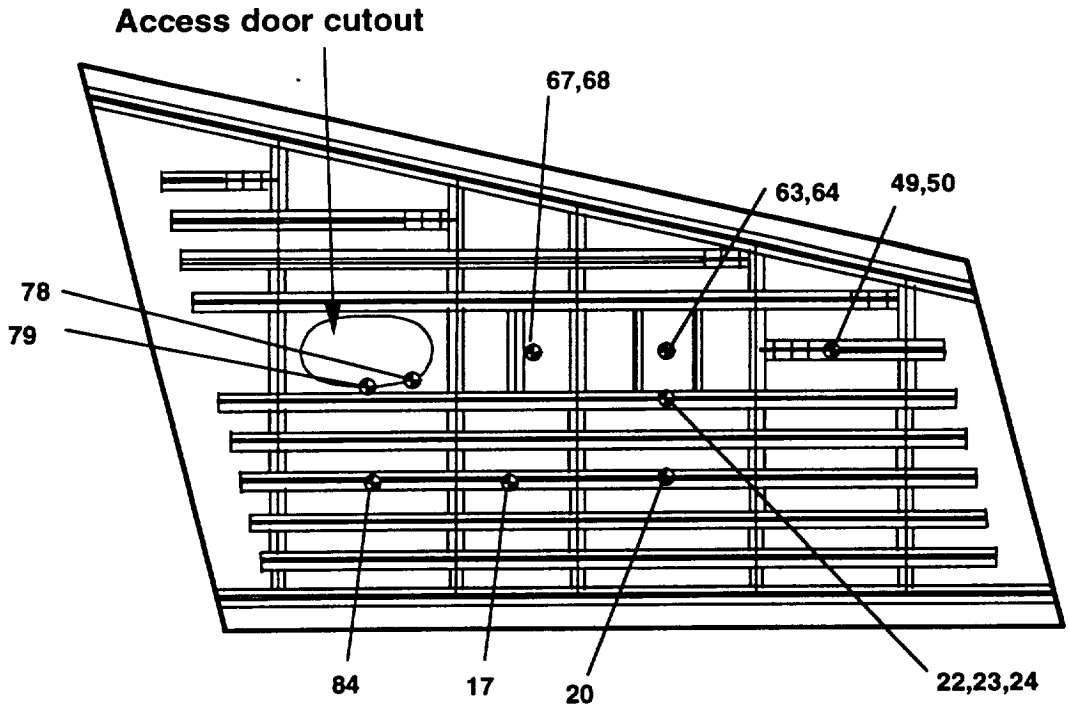

Figure 3. Upper cover and strain gage locations (gage numbers are shown on the figure).

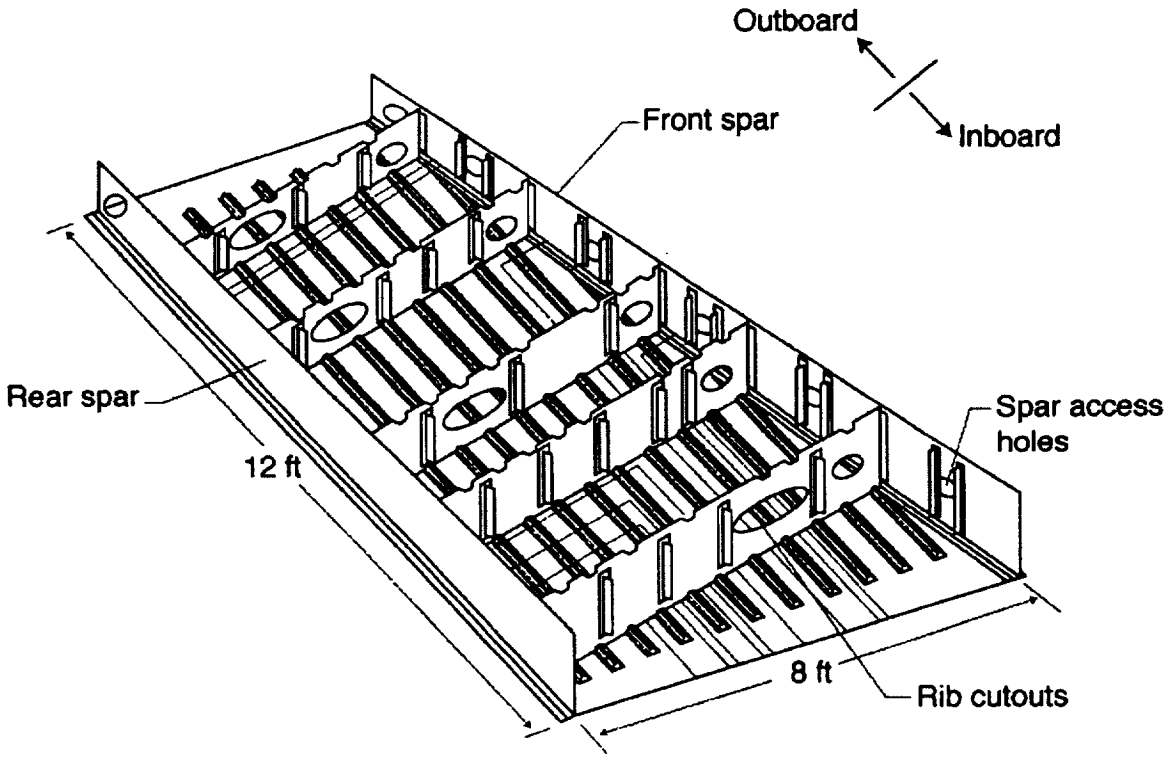

Figure 4. Interior of the composite stub box.

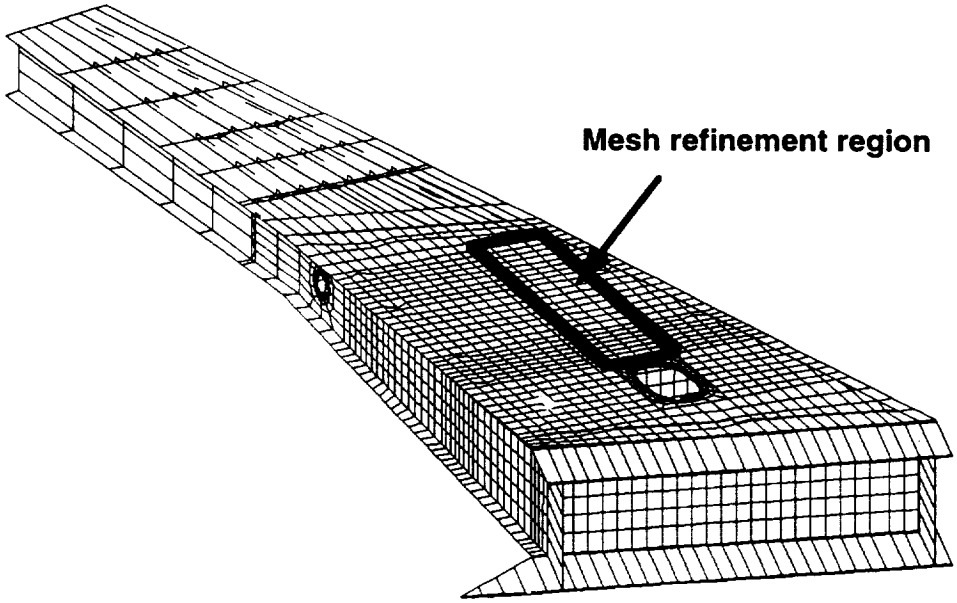

Figure 5. Finite element mesh of the initial model.

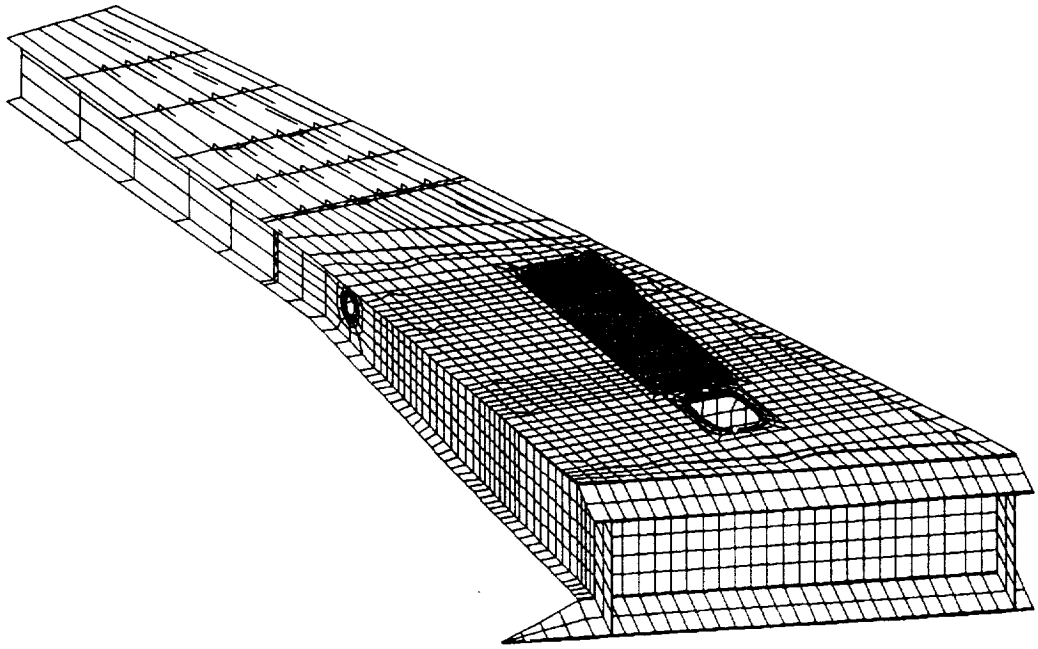

Figure 6. Finite element mesh of the the NASTRAN model.

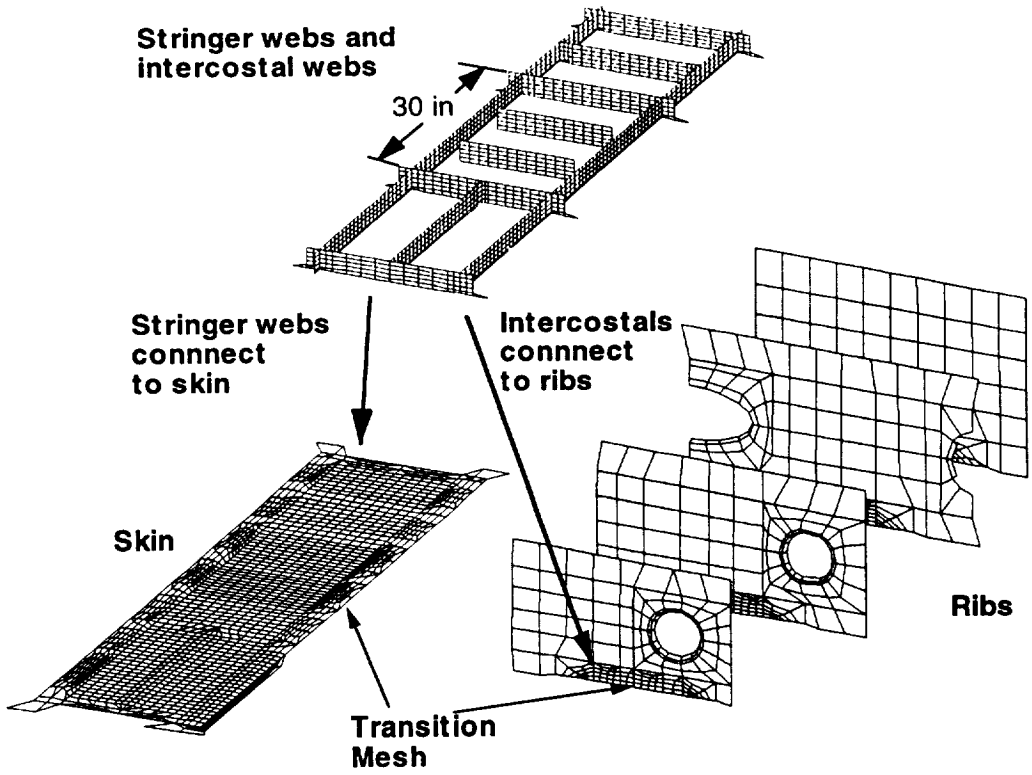

Figure 7. Mesh refinement for the skin, blade stiffeners, and intercoastals in the NASTRAN model.

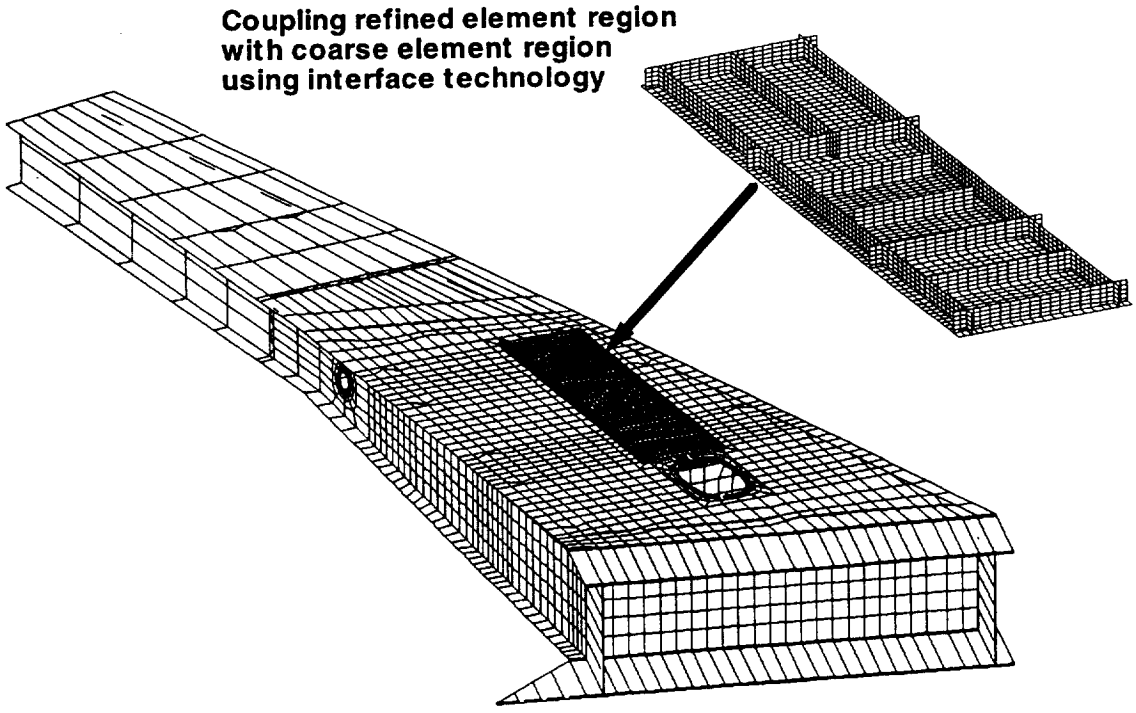

Figure 8. Finite element mesh of the interface element model.

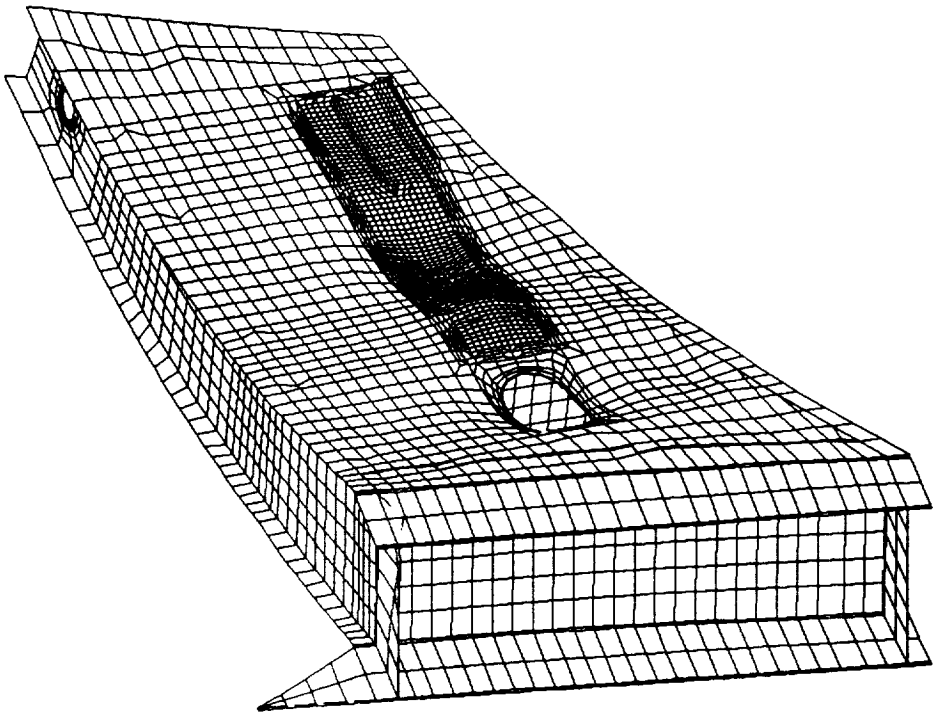

Figure 9. Deformed shape of the NASTRAN model at a load of 154 kips.

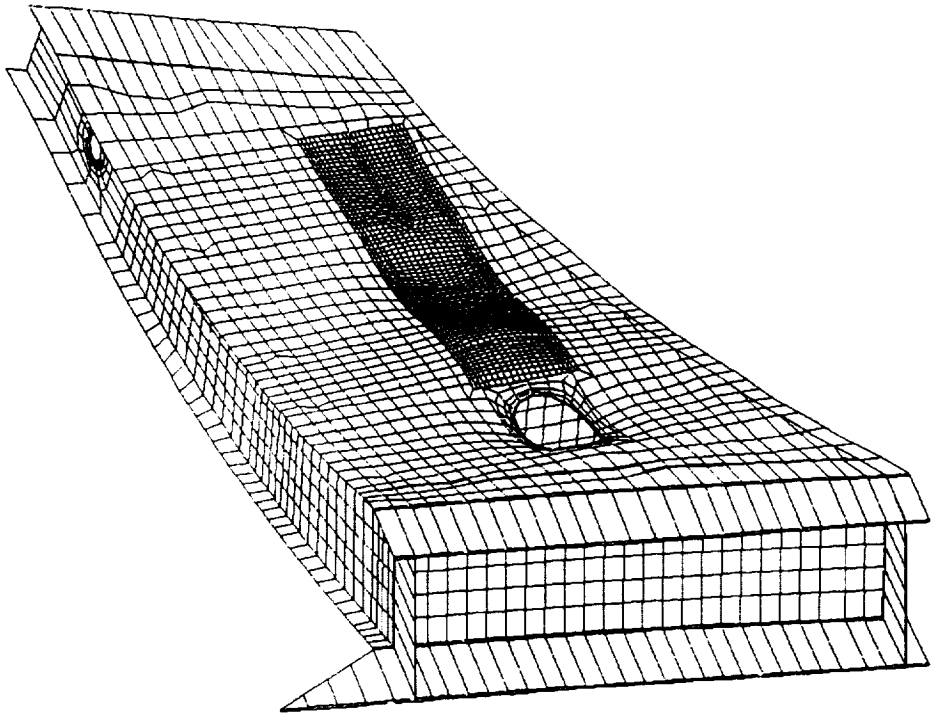

Figure 10. Deformed shape of the interface element model at a load of 154 kips.

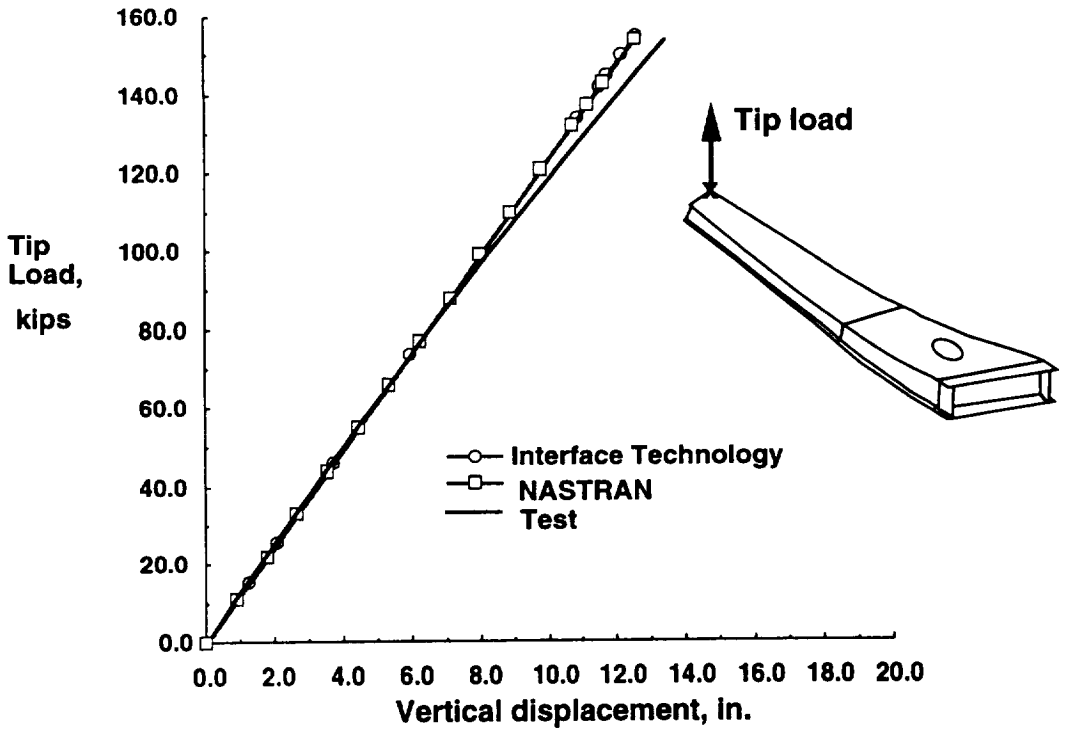

Figure 11. Stub box test article tip displacement.

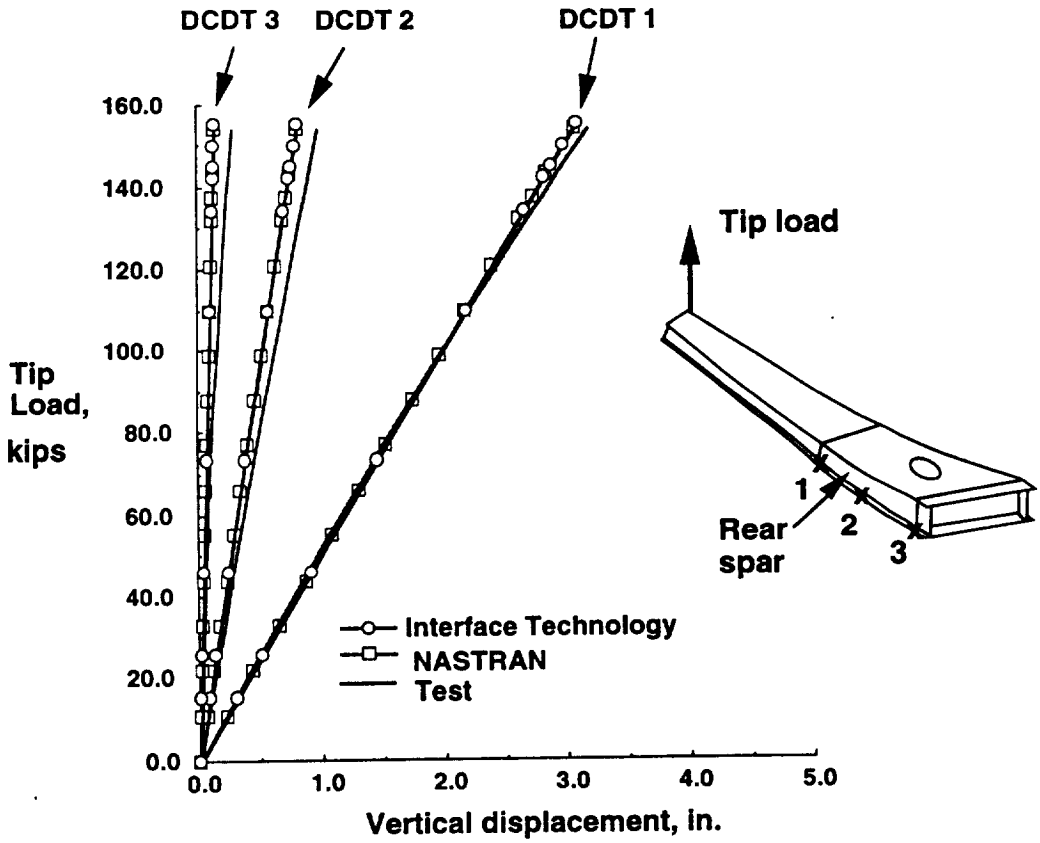

Figure 12. Vertical displacements for DCDTs 1 to 3.

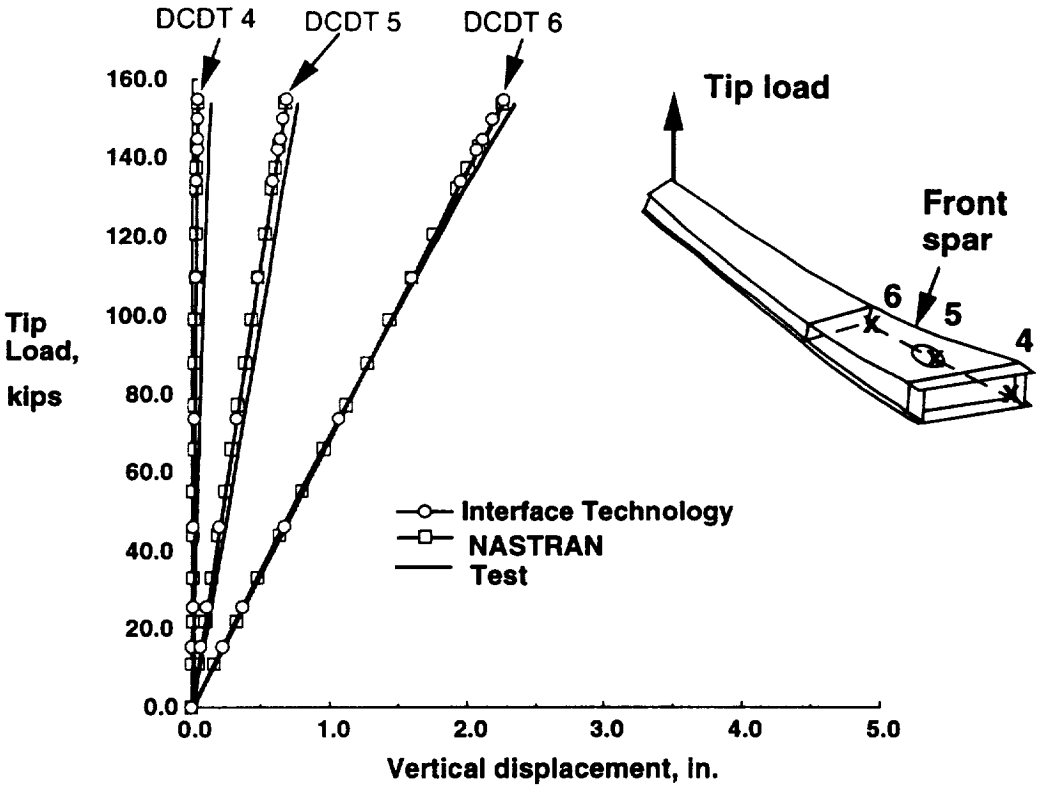

Figure 13. Vertical displacements for DCDTs 4 to 6.

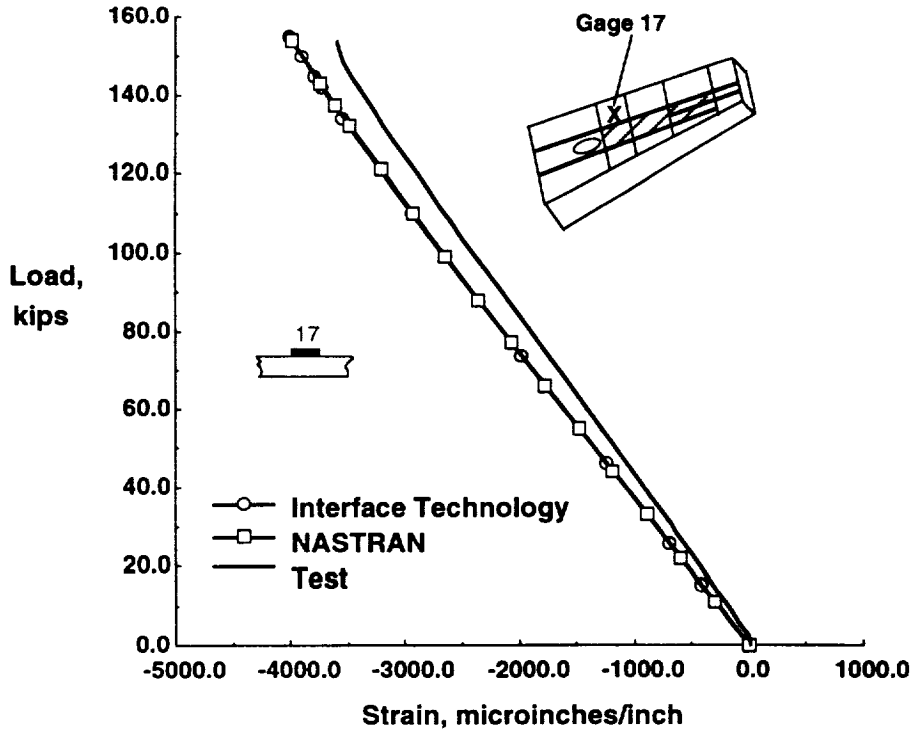

Figure 14. Correlation of far field strains for strain gage 17 on the top surface of the upper cover panel.

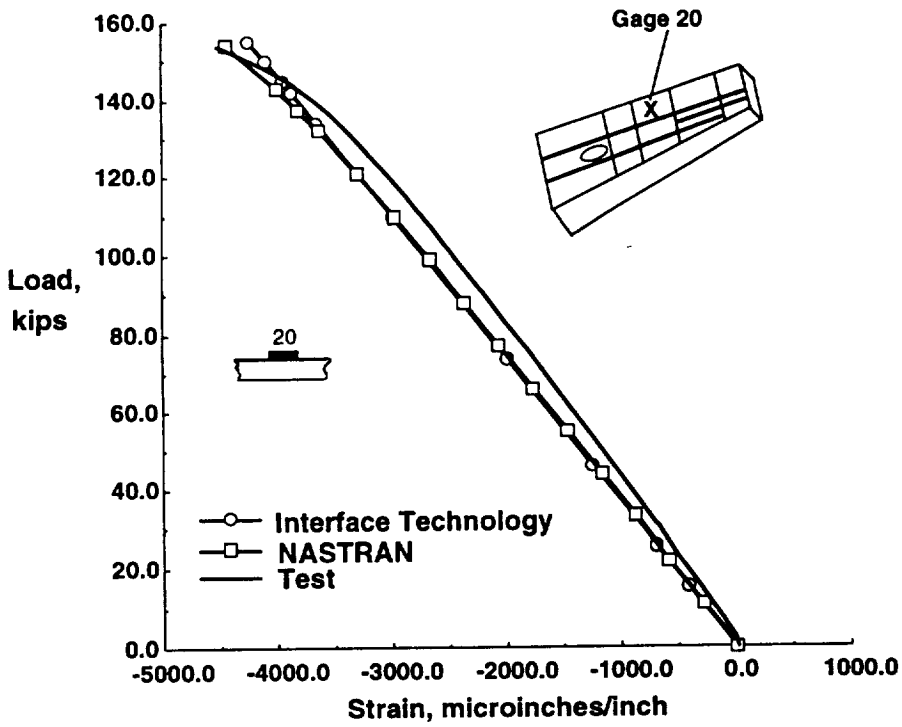

Figure 15. Correlation of far field strains for strain gage 20 on the top surface of the upper cover panel.

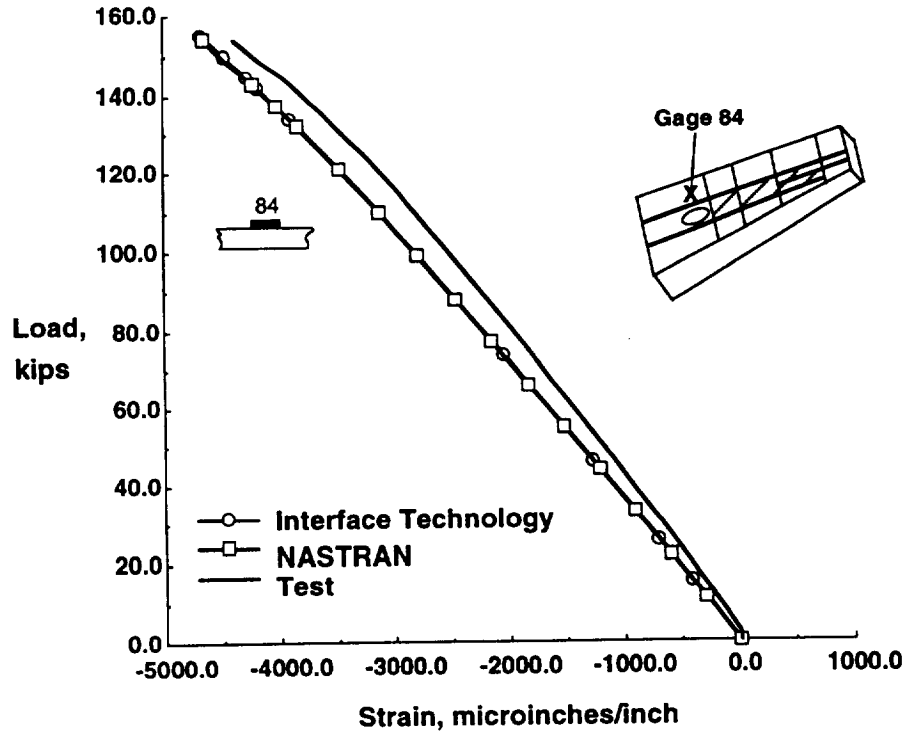

Figure 16. Correlation of far field strains for strain gage 84 on the top surface of the upper cover panel.

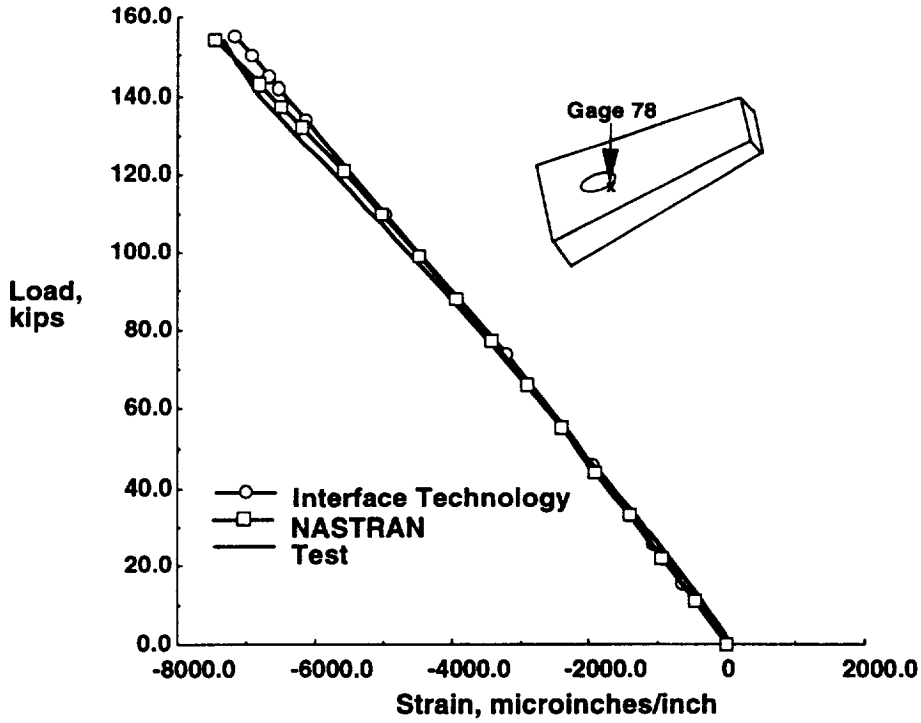

Figure 17. Correlation of strains for strain gage 78.

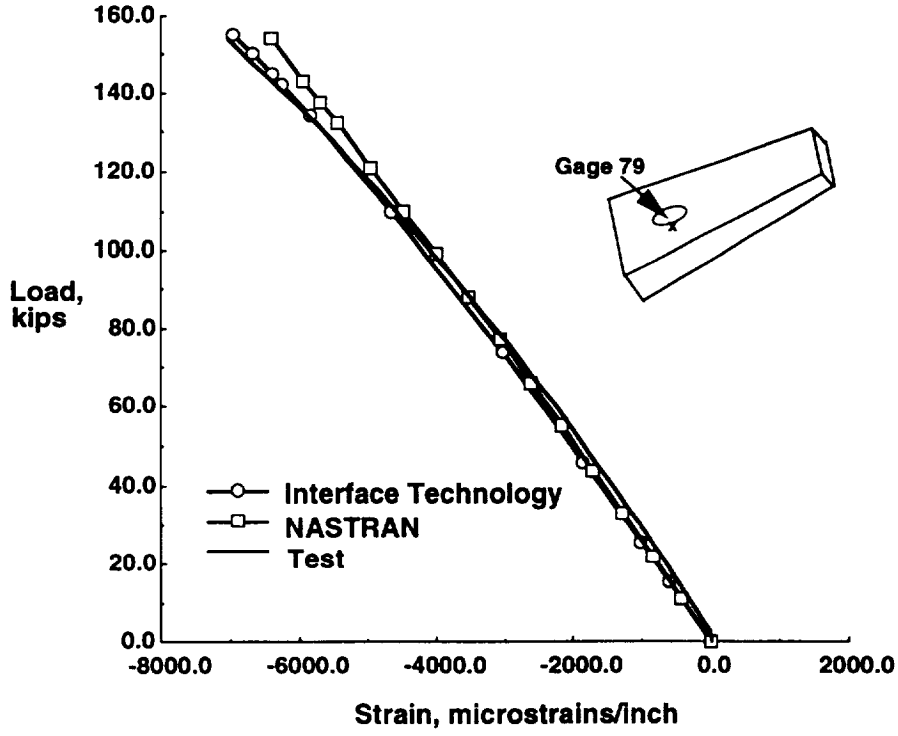

Figure 18. Correlation of strains for Gages 79.

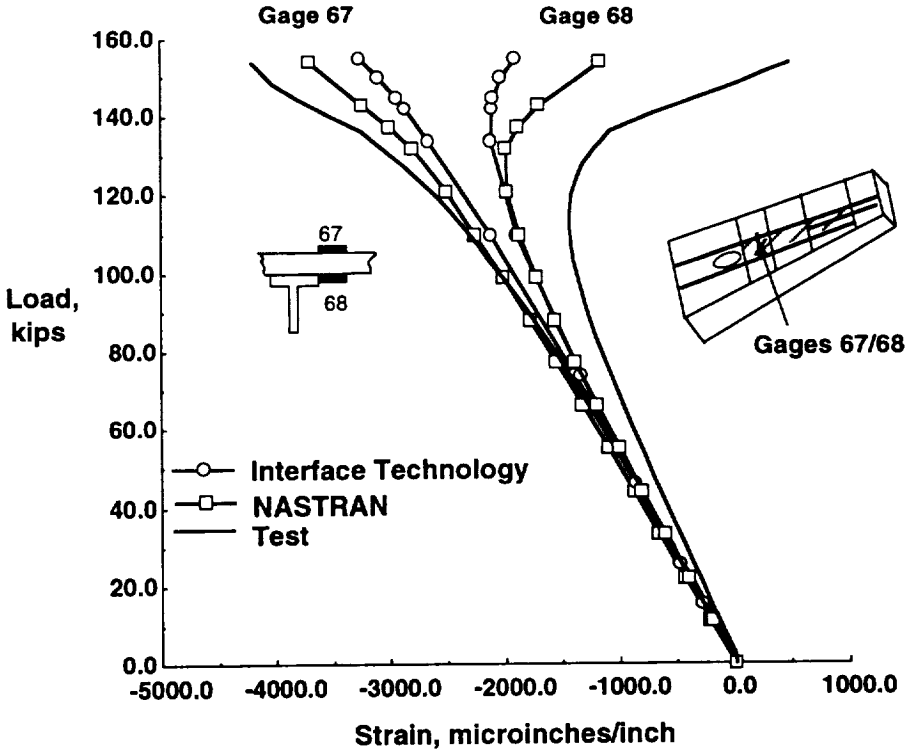

Figure 19. Correlation of strains for strain gages 67 and 68.

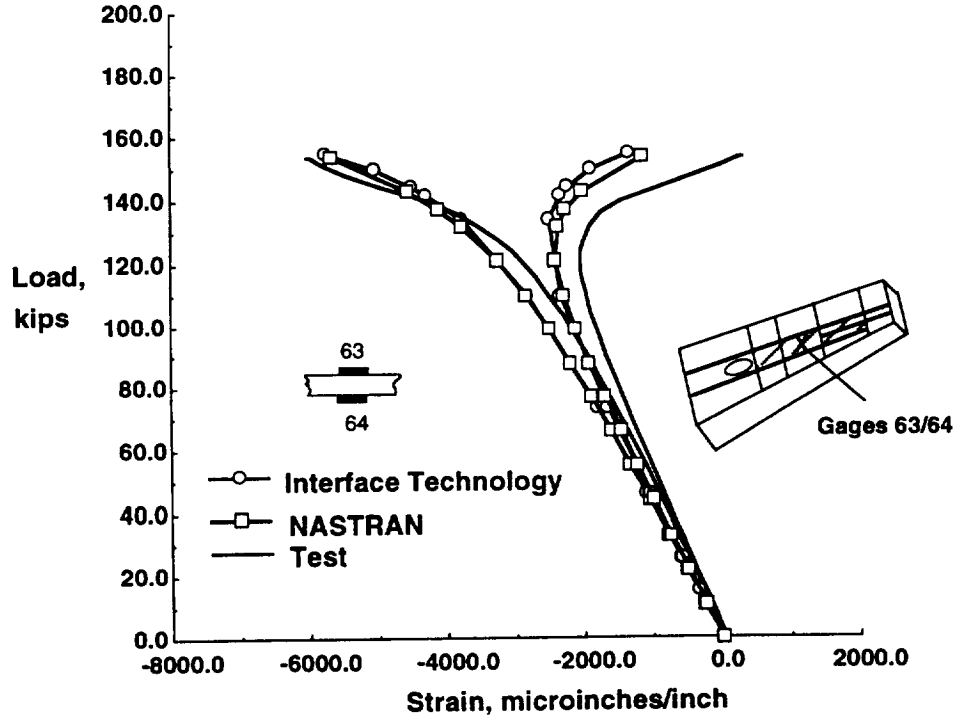

Figure 20. Correlation of strains for strain gages 63 and 64 on the upper cover panel skin.

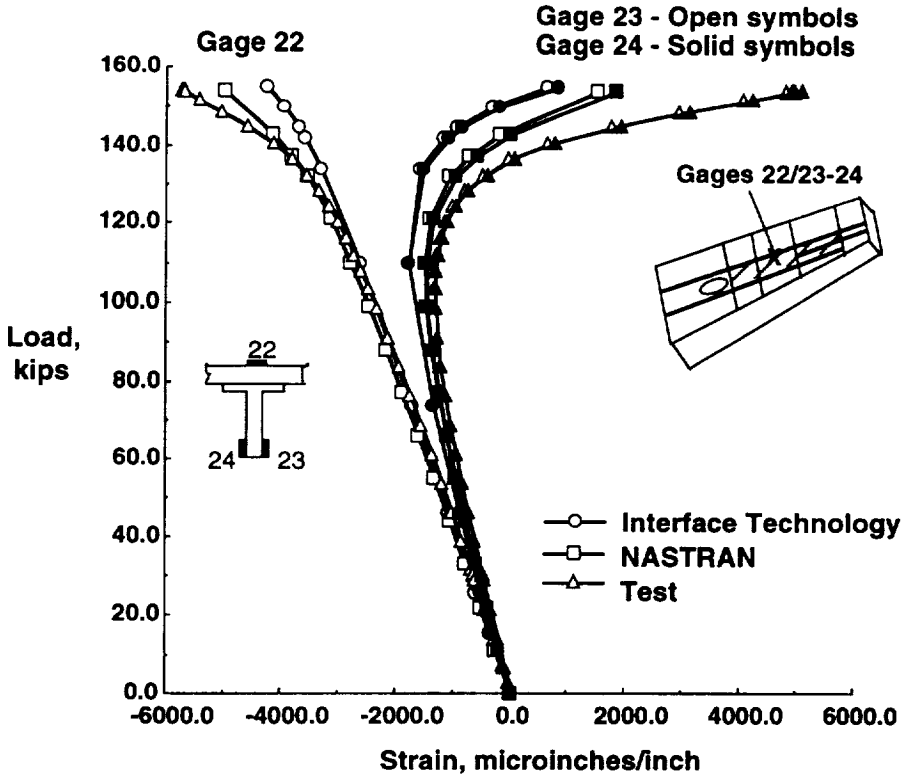

Figure 21. Correlation of strains for strain gages 22 , 23, and 24 at the aft edge of the highly nonlinearly deformed region.

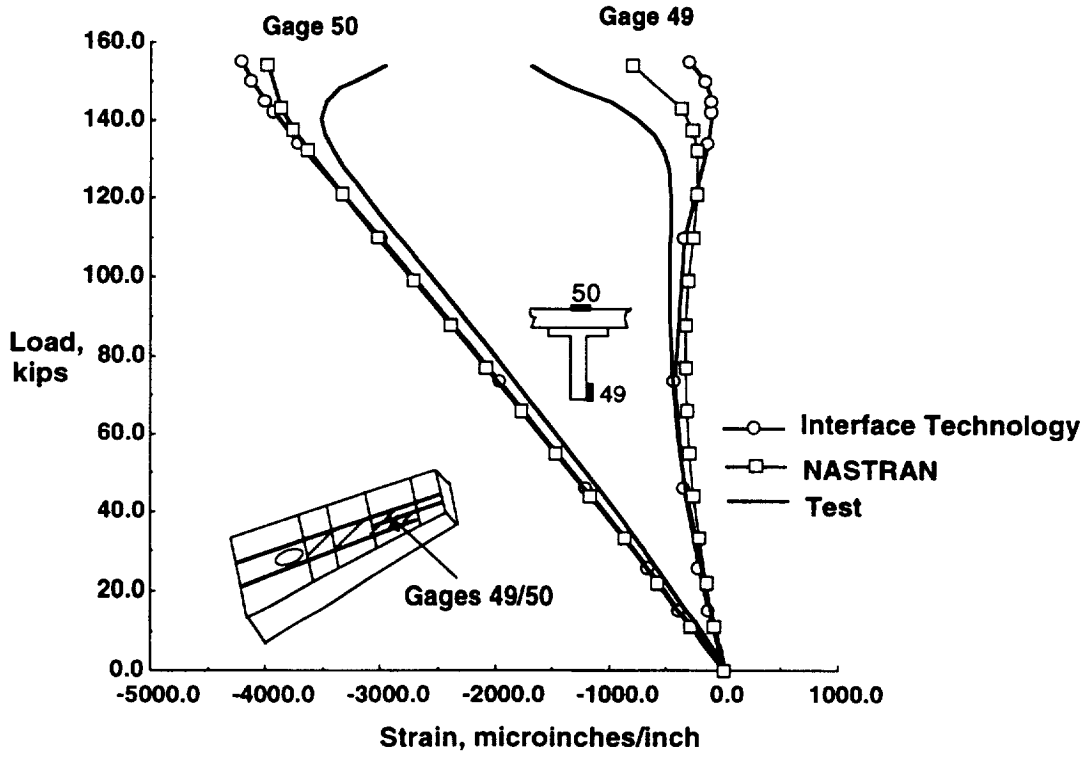

Figure 22. Correlation of strains for strain gages 49 and 50 on the runout stringer.